Direct Visualization of Macrophage-Assisted Tumor Cell Intravasation in Mammary Tumors

Jeffrey B. Wyckoff,[1,2] Yarong Wang,[2] Elaine Y. Lin,[3] Jiu-feng Li,[3] Sumanta Goswami,[2] E. Richard Stanley,[3] Jeffrey E. Segall,[2] Jeffrey W. Pollard,[3] and John Condeelis[1,2]

[1]Gruss Lipper Center for Biophotonics and Departments of [2]Anatomy and Structural Biology and [3]Developmental and Molecular Biology, Albert Einstein College of Medicine, Bronx, New York

Abstract

Although the presence of macrophages in tumors has been correlated with poor prognosis, until now there was no direct observation of how macrophages are involved in hematogenous metastasis. In this study, we use multiphoton microscopy to show, for the first time, that tumor cell intravasation occurs in association with perivascular macrophages in mammary tumors. Furthermore, we show that perivascular macrophages of the mammary tumor are associated with tumor cell intravasation in the absence of local angiogenesis. These results show that the interaction between macrophages and tumor cells lying in close proximity defines a microenvironment that is directly involved in the intravasation of cancer cells in mammary tumors. [Cancer Res 2007;67(6):2649–56]

Introduction

The tumor microenvironment plays a critical role in tumor growth and metastasis, and the stromal cells of the microenvironment are believed to directly affect the ability of tumor cells to metastasize (1–3). Macrophages in particular have been implicated in the contribution of chronic inflammation to malignancy (4), and the density of tumor-associated macrophages correlates with poor prognosis (5). It has been argued that macrophages play a direct role in the mobilization of tumor cells for metastasis (6). However, until recently, there was no direct evidence for how macrophages cause increased invasion and metastasis.

We have developed animal models that allow direct examination, by intravital multiphoton imaging, of the behavior of green fluorescent protein (GFP)-expressing carcinoma cells and stromal cells in live nondissected primary mammary tumors *in vivo* and the correlation of their behavior with metastatic potential (7–9). Intravital imaging of orthotopic rat mammary tumors has shown that increased carcinoma cell polarity and locomotion toward blood vessels correlates with increased blood burden of tumor cells and metastasis (7, 9). Further, using an *in vivo* invasion assay, involving the direct collection of invasive tumor cells into microneedles placed into the primary tumor, and multiphoton imaging, we have described a paracrine interaction between carcinoma cells and macrophages that functions in mammary tumors that is responsible for the migration of invasive tumor cells. This paracrine loop has been seen both in the orthotopic rat model and in transgenic mice with mammary tumors derived from the mammary epithelial–restricted expression of the polyoma middle T antigen (10). The paracrine loop signaling between macrophages and tumor cells is essential to the ability of tumor cells to invade within the primary tumor, involves epidermal growth factor (EGF) and colony-stimulating factor (CSF)-1 and their corresponding receptors (10), and is sufficient for invasion of collagen gels reconstituted with purified tumor cells and macrophages (11). This paracrine loop has been hypothesized to account for the involvement of macrophages in metastasis by mediating the migration of tumor cells to blood vessels, giving rise to increased intravasation (6, 10). However, the direct interaction of the invasive and migratory tumor cells with blood vessels has not been observed directly in live animals, and the involvement of macrophages, if any, has not been measured. In this study, we use multiphoton imaging of tumor cells during intravasation to determine if macrophages interact with tumor cells at the sites of intravasation *in vivo*.

Materials and Methods

Mice. All transgenic mice were crossed into a FVB-C3H/B6 mixed background and remained in a consistent background throughout breeding. Detailed origin, identification, and tumor staging of *MMTV-PyMT* and *Csf1^{op}/Csf1^{op}/PyMT* mice have been described previously (12, 13). *Csf1^{op}/Csf1^{op}/PyMT* mice have the same tumor growth rate but have delayed tumor progression compared with wild-type PyMT mice (12). *WAP-Cre/CAG-CAT-EGFP/MMTV-PyMT* (CAG-CAT-EGFP/MMTV-PyMT; ref. 14) and *Lys-GFP^{Ki}* and *c-fms (CSF-1R)-GFP* mice were described previously (15, 16). *Lys-GFP^{Ki}* and *c-fms (CSF-1R)-GFP* mice were crossed with the *MMTV-PyMT* mice to produce tumors with GFP-labeled macrophages. All genotyping was done by PCR. *Tie2-GFP* mice were described previously (17) and crossed with the *MMTV-PyMT* mice to produce tumors with GFP-labeled endothelial cells. Tumors, except where noted, were allowed to grow for 16 to 18 weeks before multiphoton imaging and blood withdrawal to ensure late-stage carcinomas and increased metastasis as described previously (12). Because the same mixed background was used for all controls and experiments, the background is not a variable.

Multiphoton imaging of macrophage populations and tumor cell migration. Multiphoton microscopy was done as described previously (9, 18). Animals were anesthetized with isoflurane, and a small incision was made in the skin to expose the tumor site without wounding the tumor or penetrating the peritoneum. The anesthetic was maintained while imaging. The tumor was imaged using a Bio-Rad (Carl Zeiss Micro Imaging Inc., Thornwood, NY) Radiance 2000 multiphoton microscope with an inverted Olympus (Olympus America Inc., Center Valley, PA) IX70 connected to a Spectra Physics Tsunami Ti:Sapphire laser. The animal was placed within a heated chamber maintained at 30°C so as to assure that both the core body temperature and imaging field temperature were maintained during imaging within the physiologic range of 34.3°C to 36.5°C. All images were collected using non-descanned detectors. The objectives used were a 20× Plan Apo 0.7NA (air) and a 60× LUMPlan/IR 0.9NA (water). The filters used were 480/30 nm and 515/30 nm (Chroma Technology Corp., Rockingham,

Note: Supplementary data for this article are available at Cancer Research Online (http://cancerres.aacrjournals.org/).

Requests for reprints: Jeffrey Wyckoff, Department of Anatomy and Structural Biology, Albert Einstein College of Medicine, 1300 Morris Park Avenue, Bronx, NY 10461. Phone: 718-430-3348; Fax: 718-430-8996; E-mail: jwyckoff@aecom.yu.edu.

doi:10.1158/0008-5472.CAN-06-1823

VT). Primary tumors (CAG-CAT-EGFP/*MMTV-PyMT, Tie2-GFP/MMTV-PyMT, MMTV-PyMT/c-fms-GFP*, or *MMTV-PyMT/lys-GFP^{Ki}* generated) were placed on an inverted microscope and imaged at 880 nm for GFP fluorescence. CAG-CAT-EGFP/*MMTV-PyMT*–generated primary tumors were imaged as above, after an injection into the tail vein of 200 μL of 20 mg/mL 70,000-kDa Texas red-dextran in Dulbecco's PBS, to load macrophages by phagocytosis 2 h before imaging.

The motility of individual tumor cells was observed as described previously (9, 18, 19). In particular, cell motility was observed by time-lapse imaging over 30 min at 1-min intervals, where a z-series was collected for each frame. Then, z-series reconstructions were made using ImageJ software to delineate single tumor cells. The distance traveled and the velocity of motility were then calculated as μm/min as described previously (7).

Macrophage pixel intensity was determined by capturing z-series of CAG-CAT-EGFP/*MMTV-PyMT*–generated tumors labeled with Texas red-dextran, with a 20× Plan Apo 0.7NA (air) objective, in which the viewing field is 512 × 512 μm and reconstructing in ImageJ. For the 60× LUMPlan/IR 0.9NA objective, a field of view is 128 × 128 μm. Pixel intensity was measured by drawing equal size boxes on a 90° view of the z-stack and averaging the pixels for each slice. Motility of tumor cells was scored as net tumor cell centroid translocation of >20 μm over 30 min of time-lapse imaging. A tumor cell was scored as moving near a macrophage if the motility occurred within 20 μm of a macrophage. Intravasation was scored as number of events per 128 × 128 × 100 = 1.6 × 10^6 μm^3 volume of tumor. All measurements were double blind scored.

Counts of perivascular macrophage clusters were done by injecting 200 μL of 20 mg/mL Texas red-dextran in Dulbecco's PBS into the tail vein of *MMTV-PyMT* and *Csf1^{op}/Csf1^{op}/PyMT* mice 2 h before imaging followed by a second injection of FITC-dextran, at the same concentration into the carotid artery to insure vessel labeling, immediately before imaging to label blood vessels. Mice were not under anesthesia for the tail vein injections but were for carotid artery injections done just before imaging. After multiphoton imaging of FITC-dextran–labeled vessels, the number of macrophages per 100 μm of vessel length in each field was counted using a double blind counter. One hundred vessels from each type of mouse were counted. Perivascular macrophage clusters were also observed in *Tie2-GFP/MMTV-PyMT* mice using similar methods.

Total numbers of macrophages were counted in whole tumor tissue using Texas red-dextran labeling and the counting method described by us previously (20).

Measuring the number of carcinoma cells in circulating blood. To measure the number of viable carcinoma cells in circulating blood from *MMTV-PyMT* and *Csf1^{op}/Csf1^{op}/PyMT* mice, animals were anesthetized with isoflurane and blood was drawn from the right ventricle of the heart using a heparin-coated 25-gauge needle and a 1-cm^3 syringe. For these experiments, +/op used as "wild-type" control animals (12) were littermates of the *Csf1^{op}/Csf1^{op}/PyMT* mice. Blood was placed in a tissue culture dish containing DMEM with 10% fetal bovine serum (FBS) and incubated overnight. The next day, the dishes were rinsed with PBS and the DMEM/10% FBS was replaced. Colonies were counted after 7 days. Each colony was scored as one tumor cell from the blood. To test the effect of PD153035, 80 mg/kg PD153035 in 8% DMSO was injected i.p. (21) into *MMTV-PyMT* mice 1 h before blood collection. One hour after injection was chosen to have a circulating concentration of PD153035 high enough to optimally block tyrosine phosphorylation. It was shown previously that phosphorylation occurs after 3 h (21). As a control, 8% DMSO was injected into identical *MMTV-PyMT* mice. To test the effect of a monoclonal anti-mouse CSF-1 receptor function blocking antibody (courtesy of Dr. S. Nishikawa, Kyoto University Medical School, Kyoto, Japan; ref. 22), 2.5 μg in 150 μL PBS were injected i.p. 4 h before blood collection. As a control, the same concentration of nonimmune IgG was injected 4 h before blood collection. Experiments were done 4 h after injection because it was determined that 4 h is required for adequate equilibration of the antibody in the extracellular space and to provide a sufficient dose of circulating antibody to neutralize the CSF-1 receptor for a 2-day period (23).

Cell collection. Cell collection using the *in vivo* invasion assay was carried out as described previously (24, 25). For testing the chemotactic response of dextran-loaded macrophages, Texas red-dextran was injected via tail vein 2 h before cell collection in both CAG-CAT-EGFP/*MMTV-PyMT* and *MMTV-PyMT/c-fms-GFP* mice. To test the efficacy of the monoclonal anti-mouse CSF-1 receptor function blocking antibody (22), 2.5 μg in 150 μL PBS were injected i.p. 4 h before cell collection.

Isolating cells from primary tumors and fluorescence-activated cell sorting. To determine if the Texas red-dextran–labeled cells were macrophages, tumors were collected from *MMTV-PyMT* and *MMTV-PyMT/c-fms-GFP* mice and dual-label fluorescence-activated cell sorting (FACS) sorted in three different ways. To isolate the macrophages from a primary tumor, a small piece of tumor was minced and filtered twice through a nylon filter to obtain a single-cell suspension and washed with PBS. First, to determine macrophages by using macrophage markers, the cells were incubated with F4/80 primary antibody for 15 min at 37°C (26) followed by R-phycoerythrin–labeled anti-rat secondary antibody (PharMingen, San Diego, CA) 1:100 for 15 min at 37°C. FACS was done based on their GFP (c-fms-GFP) expression and coexpression of F4/80 expression in macrophages using a FACSVantage cell sorter (Becton Dickinson, San Jose, CA). For Texas red-dextran–labeled cells, mice were preinjected as described above 2 h before cell sorting. Cells from the *MMTV-PyMT* tumor were isolated as above and then incubated with F4/80 primary antibody for 15 min at 37°C followed by FITC-labeled anti-rat secondary antibody (1:100 for 15 min at 37°C). FACS was done based on Texas red fluorescence and coexpression of F4/80 as detected by the FITC-labeled antibody. Third, cells from a *MMTV-PyMT/c-fms-GFP* mouse, preinjected with Texas red-dextran, were FACS sorted based on Texas red fluorescence and on their GFP (c-fms-GFP) expression. The percentage of macrophages identified with F4/80 or c-fms-GFP that costained with Texas red-dextran was calculated as a gated population with (total cells − cells only labeled with Texas red-dextran) / total cells × 100 = 97%. To determine the degree of colocalization of the Texas red-dextran–loaded macrophages with those labeled with the F4/80 antibody, a Pearson's correlation coefficient was calculated, where each element X was a pixel value from one probe and Y was the corresponding pixel of the other probe at the same spatial location and N was the number of perimeter pixels in each annulus:

$$r = \frac{\Sigma XY - \frac{\Sigma X \Sigma Y}{N}}{\sqrt{(\Sigma X^2 - \frac{(\Sigma X)^2}{N})(\Sigma Y^2 - \frac{(\Sigma Y)^2}{N})}}.$$

Real-time PCR. Quantitative reverse transcription-PCR (QRT-PCR) analysis was done to determine the change of expression of EGF in BAC1.2F5 cells cultured with or without 200 μg/mL Texas red-dextran (Invitrogen/Molecular Probes, Carlsbad, CA) for 2 h followed with or without 36 ng/mL CSF-1 (a gift from Chiron Corp., Emeryville, CA) for 4 h. PCR was done using the ABI 7900 (Applied Biosystems, Foster City, CA) with sequence-specific primer pairs for EGF as described before (11).

Results and Discussion

The identification of macrophages, tumor cells, and blood vessels. The mechanism by which the paracrine interaction between macrophages and carcinoma cells might contribute to intravasation in mammary tumors depends on the location of the two cell types relative to each other and to blood vessels (27). Tumor cells were identified by their expression of GFP from mammary epithelial–specific promoters as described previously (10). Macrophages were visualized using (*a*) i.v. injected Texas red-dextran, where tumor-associated macrophages are identified by their ability to phagocytose i.v. injected dextrans (Fig. 1*A* and *C*; Supplementary Fig. S1; ref. 28); (*b*) *MMTV-PyMT/lys-GFP^{Ki}* mice, in which the macrophages and neutrophils express GFP driven by the *lys* promoter (Fig. 1*B, top*); and (*c*) *c-fms (CSF-1R)* promoter-driven GFP-expressing mice, in which monocytes and macrophages express GFP driven by the *c-fms* promoter (Fig. 1*B, bottom*; ref. 16, 17). FACS sorting of Texas

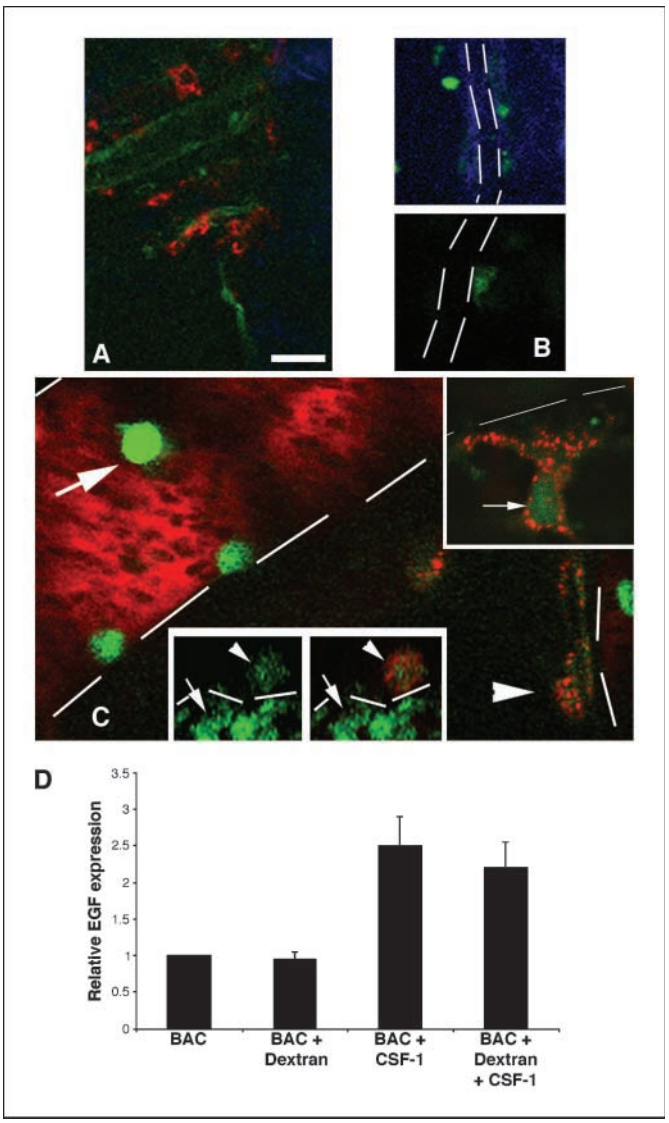

Figure 1. Identification of tumor-associated macrophages in mammary tumors in live animals. *A,* multiphoton microscopy of Texas red-dextran–labeled macrophages (*red*) in living *MMTV-PyMT/Tie2-GFP* tumors (*green endothelial cells*) was done to observe the location of macrophages relative to blood vessels. Macrophages were observed in the stroma subluminal to endothelial cells lining the blood vessels in a cross-optical section. The collagen matrix (*blue*) is imaged by second harmonic generated polarized light. *Bar*, 25 μm. An en face section is shown in Supplementary Fig. S1. *B,* GFP-labeled macrophages (*arrows*) are seen in the subluminal wall of blood vessels (*dashed lines* define the vessel walls) present in either a *Lys-GFP* × *MMTV-PyMT* mouse (*top*) or a *c-fms-GFP/MMTV-PyMT* mouse (*bottom*), in which the macrophages are GFP positive and tumor cells are unlabeled and appear as black regions. Collagen matrix (*blue*) is imaged by second harmonic generated polarized light. *C, lys-GFP*–labeled macrophages that are in the subluminal stroma take up Texas red-dextran and are green and red, whereas monocytes in the blood do not and are only green. Macrophages (*arrowhead*) are seen outside dextran-labeled vessels (*red*, blood space), whereas monocytes (*arrow*) are seen in the blood vessel but do not take up dextran. *Bottom paired insets,* the same result was seen in *c-fms-GFP* mice. *Left inset,* all GFP-expressing cells (*green channel* only); *right inset,* same field (*green* and *red channels*) with a macrophage having taken up Texas red-dextran by phagocytosis 2 h after tail vein injection. The monocytes are not labeled with Texas red-dextran. *Arrows,* monocytes; *arrowheads,* macrophages. *Top inset,* high-magnification image of a macrophage loaded with Texas red-dextran subluminal to a vessel. *Dashed lines,* delineate blood vessel walls in both (*C*) and insets. *D,* dextran loading of macrophages does not affect EGF production by macrophages. QRT-PCR shows a 2-fold increase of mRNA production of EGF after CSF-1 stimulation whether the macrophages have been preloaded with dextran or not (there is no significant difference by standard *t* test between dextran-containing and nondextran-containing samples).

red-dextran–loaded cells from primary tumors showed that >97% of dextran-loaded cells were positive for the macrophage-specific markers F4/80 and c-fms-GFP expression (Supplementary Fig. S2). Furthermore, correlation analysis of the FACS-sorted macrophages for F4/80 and Texas red-dextran gave a Pearson's coefficient of 0.87. FACS quantitation showed that almost all macrophages were labeled with Texas red-dextran, indicating that there is no significant population of macrophages that is not loaded with Texas red-dextran.

In both *lys-GFP* and *c-fms-GFP* mice with MMTV/PyMT-derived tumors, cells in the blood flow within vessels were not labeled with dextran, whereas 100% of tumor stroma–associated cells were labeled with dextran (Fig. 1*C*). This is interesting because all GFP-expressing blood-borne cells in *c-fms-GFP* mice are of the monocytic lineage by staining with F4/80 antibodies (26). In *lys-GFP* mice, GFP-expressing blood-borne cells are monocytes and granulocytes (16). These results indicate that macrophages phagocytose dextran only when in the stroma of the primary tumor and not while flowing in the blood.

To determine if macrophages in the stroma of mammary tumors after dextran loading were still active in paracrine-mediated invasion (24), the *in vivo* invasion assay was used to collect invading tumor cells and macrophages from mice with *MMTV-PyMT/c-fms-GFP* tumors 30 min after i.v. injection of Texas red-dextran. Under these conditions, 100% of the invading macrophages accompanying tumor cells were loaded with Texas red-dextran and collected in the same numbers as from control tumors in animals not preinjected with Texas red-dextran. This indicates that the EGF/CSF-1 paracrine loop remains functional after phagocytosis of Texas red-dextran by macrophages and that macrophages throughout the volume of the primary tumor were Texas red-dextran labeled. This result was consistent with the ability of macrophages to produce EGF after CSF-1 stimulation even when dextran loaded (Fig. 1*D*).

To investigate the relative locations of tumor cells and macrophages to blood vessels, multiphoton microscopy of CAG-CAT-EGFP/*MMTV-PyMT* mice (mice with GFP-expressing tumor cells) was done as described previously (10, 14). Macrophages were identified by Texas red-dextran loading. Blood vessels were unequivocally identified using (*a*) i.v. injected fluorescent dextrans to label the blood space immediately before imaging (Fig. 1*C*), (*b*) light scattering from erythrocytes in blood vessels in the absence of dextrans, and (*c*) multiphoton imaging of mice with *MMTV-PyMT/Tie2-GFP* tumors in which endothelial cells express GFP from the *tie2* promoter (Fig. 1*A*; Supplementary Fig. S1; ref. 17). Multiphoton microscopy of mice with *MMTV-PyMT/Tie2-GFP* tumors in which endothelial cells express GFP from the *tie2* promoter, and of macrophages labeled by their ability to phagocytose i.v. injected Texas red-dextran (28), shows that the perivascular macrophages are located adluminal within the stroma of the tumor and not luminal within the blood space of the vessel (Fig. 1*A*; Supplementary Fig. S1).

Interactions between macrophages, tumor cells, and blood vessels leading to intravasation in mammary tumors. Using the methods to unequivocally label all macrophages in living tumors described above, multiphoton microscopy showed that macrophages are present in large numbers at the margin of the tumor and then decreasingly throughout the stroma as one imaged deeper inside the tumor (Fig. 2*A*). In the center of the tumor where most of the blood vessels are located, many macrophages were found in association with blood vessels. The same distribution of

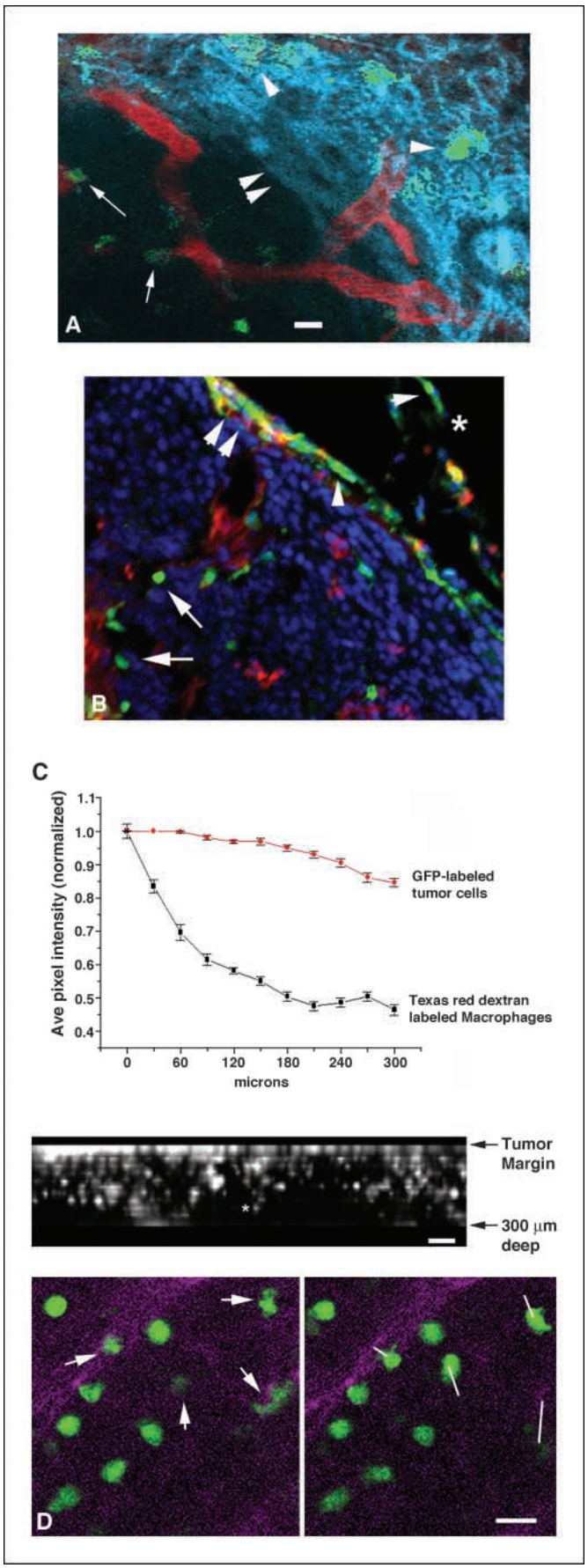

macrophages was seen in histologic sections of primary tumors from identical mice, although the tumor volume was collapsed due to dehydration (Fig. 2*B*). The density of macrophages per unit volume of tissue decreased from the tumor margin to the deeper regions of the tumor where many perivascular macrophages were seen (Fig. 2*C, bottom*). This decrease in macrophage density was not due to loss of fluorescence detection efficiency because tumors with GFP-expressing tumor cells showed excellent fluorescence intensity to the same depth of imaging as that used for macrophages (Fig. 2*C*). Perivascular macrophages were best imaged by multiphoton microscopy and not by conventional confocal microscopy in undissected tumors because most perivascular macrophages reside deep within the tumor beyond the depth of imaging of pinhole confocal microscopy. This same distribution pattern of macrophages was seen in tumors using all three methods described above for visualizing macrophages (Lys-GFP^{Ki}, c-fms-GFP, and fluorescent dextran phagocytosis), consistent with the results described above that all three methods detected macrophages equally well. Furthermore, the density of tumor-associated macrophages seen with Texas red-dextran labeling was the same as observed using anti-F4/80 immunohistochemistry (20).

High-resolution imaging of perivascular macrophages showed that they are associated with vessels both as single motile macrophages (Fig. 2*D*) and as clusters (Figs. 3*C* and 4*A*). Macrophage clusters have been described previously in invasive regions of human tumors (29, 30). To determine the average number of macrophages in each perivascular cluster seen in the animal models used here, z-series images were projected in stereo (data not shown) to count the number of macrophages in each perivascular-associated GFP-positive or Texas red-dextran–positive region. The results indicate that perivascular macrophages can be found as individual cells and as clusters, where each cluster contains an average of 3 $\pm$ 0.5 macrophages (SE; n = 40).

Figure 2. Tumor-associated macrophages are found in the tumor margin and as a perivascular population deep within mammary tumors. *A,* in living undissected tumors, GFP-labeled macrophages are seen in the tumor margin (i.e., the connective tissue surrounding the tumor) and as perivascular macrophages (*arrows*) associated with the microvasculature (*red*) deep within the tumor as seen in a *Lys-GFP* $\times$ *MMTV-PyMT* mouse, in which the tumor cells are unlabeled and appear as *black regions*. The stroma of the tumor margin is filled with collagen fibers (*light blue*) as imaged by second harmonic generated polarized light by the multiphoton microscope and appears as a bright layer around the tumor (*double arrowhead* points to the interface between the tumor and the tumor margin). *Arrowheads,* macrophages found in the tumor margin are associated with this collagen layer. *Bar,* 25 μm. *B,* the same tumor morphology and macrophage density is seen in histologic section (although collapsed due to fixation and dehydration) of a late-stage carcinoma in a *MMTV-PyMT/c-fms-GFP* mouse. Macrophages (*green*) are seen at the tumor margin (*arrowheads*) and as perivascular macrophages (*arrows*). The tumor is stained with 4′,6-diamidino-2-phenylindole (*blue*) and the vessels are filled with Texas red-dextran (*red*). *Asterisk,* the outside edge of the tumor margin. *C,* macrophage density per unit area falls off rapidly from the tumor margin toward the center of the tumor. This is not due to loss of imaging efficiency because pixel intensity from the GFP-labeled tumor cells remains above 85% through the same 300 μm distance. Pixel intensities from thirty 10-μm-thick z-sections, as illustrated as a stack of images in the x-z projection at the bottom of the figure, were quantified to show differences in macrophage density. *Bottom,* x-z projection of thirty 10-μm-thick optical sections with the first section starting at the tumor margin (*arrow, Tumor margin*) and extending 300 μm deep into the undissected tumor (*arrow, 300 μm deep*). Single spots (*asterisk*) in the x-z projection are the perivascular macrophages. *Bar*, 100 μm. *Points*, mean (n = 20); *bars*, SE. *D,* perivascular macrophages (*green*) are seen crawling at the surface of a blood vessel (delineated by *white line* in *left*) and along matrix fibers (*purple*) in the stroma around the vessel in a living tumor in a *MMTV-PyMT/lys-GFP* mouse. Time-lapse images taken 5 min apart show the movement of macrophages (*left, arrows*). *Right, lines,* track distance traveled by macrophages over 30 min. *Bar*, 25 μm.

In the *PyMT* tumors, the motility of individual tumor cells was imaged as described previously (18, 19). Using these methods in *PyMT* tumors, the motility of tumor cells was observed to occur >80% of the time near macrophages, at the tumor margin, deep within the primary tumor and in association with perivascular macrophages (Fig. 3*A*), consistent with the paracrine interaction between the two cell types reported previously to induce cell motility (10). The absolute number of tumor cell motility events observed per hour is greater at the tumor margin compared with the perivascular region, but when the frequency of tumor cell motility is normalized to macrophage density, tumor cell motility is much more frequent adjacent to perivascular macrophages (Fig. 3*B*). Tumor cells were seen migrating directly toward macrophages (Fig. 3*C, bottom*; Supplementary Movie 1). Tumor cell speed during motility associated with perivascular macrophages was 3.9 $\pm$ 0.28 μm/min (SE; n = 20 cells from eight different animals). The migration of tumor cells directly toward macrophages is an interesting observation because, although tumor cell motility at the tumor margin is believed to be related to invasion of the primary tumor mass into normal tissue, tumor cell motility associated with perivascular macrophages is correlated with intravasation (Figs. 3*C* and 4).

To determine if perivascular macrophages are the sites of intravasation of tumor cells in *PyMT* tumors, mice with GFP-expressing tumor cells were i.v. injected with Texas red-dextran to label macrophages and then time-lapse imaged to observe if the intravasation of GFP-expressing tumor cells is either near or distant from the perivascular macrophages. A 1.6 $\times$ 10^6–μm^3 volume of tumor containing a blood vessel and at least one macrophage was selected at random and time-lapse imaged for 30 min to score intravasation. Time-lapse imaging showed that tumor cells migrate toward the vessel-associated macrophages and become closely associated with the vessel surface (Fig. 3*C*; Supplementary Movie 1). In addition, tumor cells were seen to intravasate only where perivascular macrophages were present (Supplementary Fig. S3 and Fig. 4*A*; Supplementary Movies 2 and 3). The intravasation events scored live by time-lapse imaging (18 events in 96 volumes in 19 animals) always occurred within 20 μm of a macrophage (Supplementary Movie 4 shows the intravasation and disappearance of tumor cells as they are swept away in the blood flow). z-series analysis of the site of intravasation confirmed the presence of a macrophage above or below the plane of imaging even if not seen in the same plane of focus as the tumor cell, indicating that in all cases a macrophage was within one cell diameter of the intravasating tumor cell.

To determine if intravasation efficiency is related to the density of perivascular macrophages, *Csf1^{op}/Csf1^{op}/PyMT* mice defective in CSF-1 production were used. These mice show tumor growth like wild-type and +/op animals but slower tumor progression and decreased invasion and metastasis consistent with the requirement for CSF-1 signaling for invasion and metastasis and the observed lower densities of tumor-associated macrophages in *Csf1^{op}/Csf1^{op}/PyMT* mammary tumors (20, 31). Therefore, we investigated the relative number of perivascular macrophages in +/op *MMTV-PyMT* and *Csf1^{op}/Csf1^{op}/PyMT* tumors in animals from the same litter and found that the *+/op/PyMT* tumors had more than six times as many perivascular macrophages per 100 μm length of blood vessel (Fig. 4*B*). To determine if intravasation efficiency is correlated with the number of perivascular macrophages, the number of viable tumor cells circulating in the blood was determined by drawing blood from the right ventricle of the heart directly downstream from the mammary tumor, thereby avoiding intervening capillary

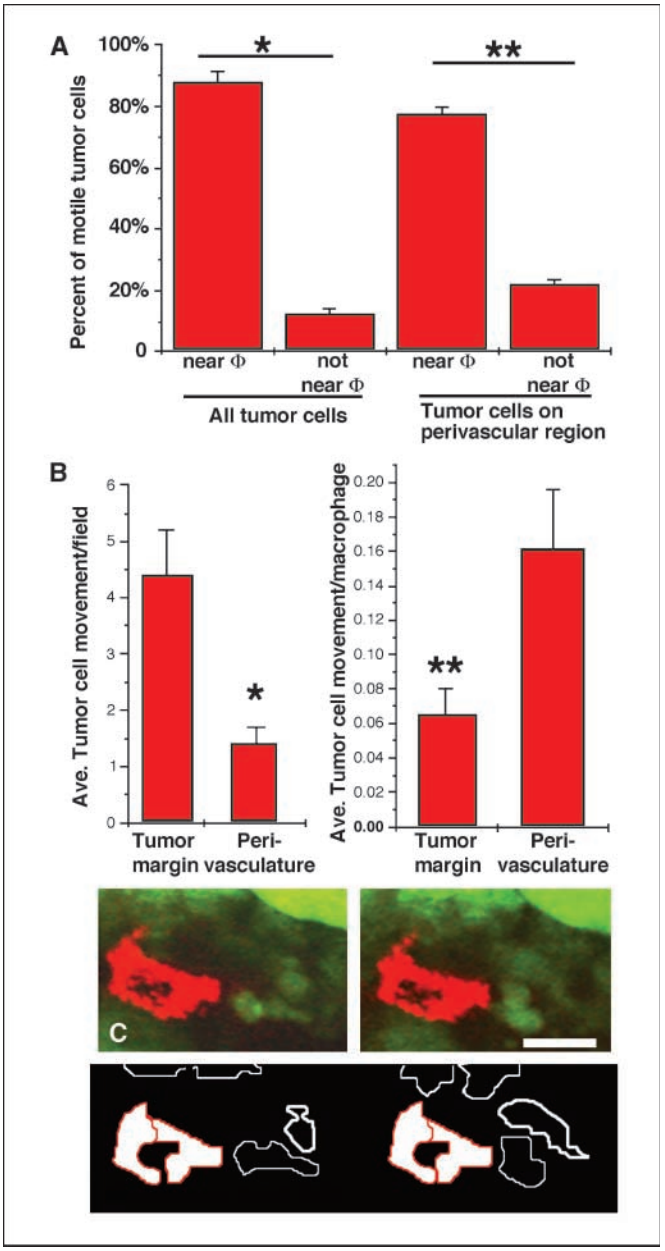

Figure 3. Tumor cell motility occurs most frequently in association with perivascular macrophages. *A,* tumor cells were seen to move most frequently in association with macrophages in both the tumor margin and the perivascular region. Tumor cell movement was scored to be in association with a macrophage when it occurred within 20 μm (one cell diameter) of a macrophage. Movements of tumor cells in both the tumor margin and perivascular regions = all tumor cells. Movement in association with perivascular macrophages = tumor cells in perivascular region. *Columns,* mean (n = 12 animals, 28 z-series); *bars,* SE. *, P = 0.0036; **, P = 0.0002, comparing near and not near. *B,* although the absolute number of tumor cells moving at the tumor margin was greater, as shown in left, a higher frequency of tumor cell movement was observed in association with perivascular macrophages when movement was normalized to the number of macrophages per unit area (*right*). Numbers were obtained by counting cell movements and the number of macrophages for volumes in the tumor margin of 512 $\times$ 512 $\times$ 60 μm and for identical volumes in the region of tumor containing the microvasculature. *, P = 0.0018; **, P = 0.0064, comparing tumor margin and perivascular. *C,* images from a 30-min time-lapse sequence, taken at 6-min intervals, of four GFP-labeled tumor cells (*green*) in a PyMT-generated mammary tumor CAG-CAT-EGFP/*MMTV-PyMT* in a living animal moving in association with a macrophage cluster containing two macrophages (*red*) near a vessel. The tumor cells move at a rate of 4.2 μm/min over the course of the 30-min time-lapse. Tumor cell motility is defined in Materials and Methods. *Bottom drawing,* outline of the tumor cells (*white outlines*) as they move toward the macrophages (*filled*). *Bar*, 25 μm.

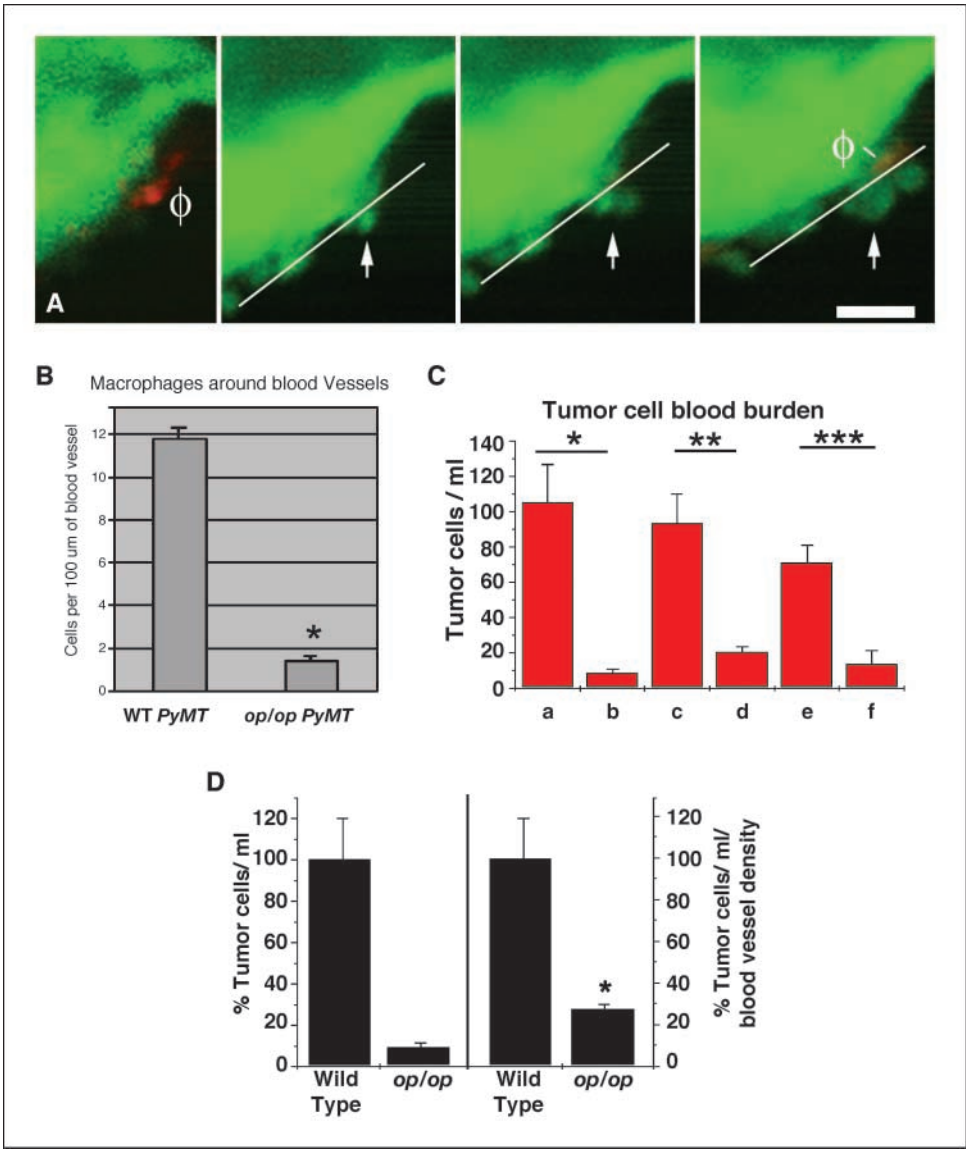

Figure 4. Perivascular macrophages are sites of EGF-dependent and CSF-1–dependent intravasation in PyMT mammary tumors. *A,* image from a z-series time-lapse sequence taken at 8-min intervals of a cell entering a vessel in association with a macrophage. *Left,* subluminal macrophage (ϕ) in the first frame of the time-lapse movie 10 μm below the plane of focus of the other panels; *middle left,* a different plane of focus at the same time frame as the left. *Middle left, middle right,* and *right,* same plane of focus and the movement of tumor cells into the vessel. *Line,* vessel wall; *arrow,* point of intravasation of tumor cells. ϕ, position of the macrophage in the first frame. By the last frame, the macrophage (ϕ), which started out 10 μm below the plane of focus, has moved into the same plane as the intravasating tumor cells. This indicates that both tumor cells and macrophages are motile at the vessel surface. *Bar*, 25 μm. *B,* more perivascular macrophages are seen along blood vessels in +/op wild-type (*WT*)-like *PyMT* mouse mammary tumors than in *Csf1^{op}/Csf1^{op}* × *PyMT* mammary tumors. Macrophages were labeled by injection of Texas red-dextran and then counted along vessels. Macrophage density was >6-fold higher in *+/op/PyMT* mouse mammary tumors than in *Csf1^{op}/Csf1^{op}* × *PyMT* mammary tumors. *, $P = 0.0003$. *C, a* and *b,* the number of viable tumor cells in the blood exiting the primary tumor (blood burden) is greatly reduced in *Csf1^{op}/Csf1^{op}* × *PyMT* tumor-bearing mice (*b*) compared with *+/op/PyMT* mice (*a*). *, $P = 0.0002$ ($n = 8$). *c* and *d,* in addition, the blood burden is greatly reduced 1 h after the injection of 80 mg/kg PD153035 in wild-type mice (*d*), which inhibits the activity of the EGF receptor ($n = 8$). *c,* control mice injected with 8% DMSO. **, $P = 0.0005$. *e* and *f,* the blood burden also is greatly reduced 4 h after the injection of anti-CSF-1 receptor function blocking antibody (2.5 mg/mL) in wild-type mice (*f*; $n = 6$). *e,* wild-type mice i.p. injected with nonimmune IgG. ***, $P = 0.0002$. *D,* on normalizing the numbers of cells collected from the blood to the vascular density of late-stage carcinoma tumors from *+/op/PyMT* mice compared with *Csf1^{op}/Csf1^{op}* × *PyMT* mice, there is a 4-fold difference in the number of cells collected. *, $P = 0.002$.

beds that might trap tumor cells. The results show that *+/op/PyMT* mice with 6-fold more perivascular macrophages had 16-fold more viable tumor cells per mL of blood than *Csf1^{op}/Csf1^{op}/PyMT* mice with few perivascular macrophages (Fig. 4*B* and *C, columns a* and *b*). To compensate for differences in vascular density between the *+/op/PyMT* and *Csf1^{op}/Csf1^{op}/PyMT* mice, the numbers of cells collected from the blood were normalized to the vessel density of primary tumors from wild-type and *Csf1^{op}/Csf1^{op}* mice (Fig. 4*D*; ref. 20). The number of tumor cells in the blood of *Csf1^{op}/Csf1^{op}* animals remained significantly reduced compared with that in *+/op* animals when the data were normalized to vessel density (Fig. 4*D*). These results indicate that it is the number of perivascular macrophages and not the number of blood vessels that correlates with intravasation.

In previous studies using an *in vivo* invasion assay, a paracrine loop was identified between carcinoma cells and macrophages,

where tumor cell EGF receptors and macrophage CSF-1 receptors are signaled by macrophage-produced EGF and tumor cell–produced CSF-1, respectively, leading to chemotaxis-mediated comigration and invasion of both cell types (10). To test the hypothesis that this paracrine signaling loop, involving EGF and CSF-1 receptors, is involved during the intravasation of carcinoma cells at perivascular macrophage clusters, EGF receptor activity was inhibited by i.p. injection of 80 mg/kg PD153035, an erbB1 and erbB2 receptor tyrosine kinase inhibitor. This concentration of PD153035 correlates to 15 μmol/L in the blood plasma after 1 h (21). One hour after injection of PD153035, the number of tumor cells exiting the primary tumor in the blood dropped by 5-fold in *MMTV-PyMT* mice treated with PD153035 compared with controls mock injected with buffer (Fig. 4*C, columns c* and *d*).

To determine if the CSF-1 receptor activity is also essential for intravasation, we injected i.p. 2.5 mg/mL of monoclonal antibody that is function blocking for CSF-1 receptor activity (22). Four hours after i.p. injection, the time of peak inhibition of receptor activity (23), the number of tumor cells found in the blood was 6-fold less than MMTV-PYMT mice injected with nonimmune IgG (Fig. 4*C, columns e* and *f*).

To confirm that the antibody blocked the paracrine loop described previously (10), the *in vivo* invasion assay was done 4 h after i.p. injection into 18-week-old *PyMT* × *c-fms-GFP* tumor-bearing mice. The number of collected cells per needle (tumor cells plus macrophages) from needles containing 25 nmol/L EGF was ~1,000 total cells on average (75% tumor cells and 25% macrophages) from mice with control antibodies but reduced to 127 ± 48 total cells (3% macrophages) from mice injected with CSF-1 receptor function blocking antibody. These numbers are very similar to what was seen when the same antibody was placed in the needle during the invasion assay (10), showing the inhibition of CSF-1-receptor activity in the tumor following i.p. injection of the function blocking antibody as used in the current study.

In total, these experiments show that intravasation follows the same pattern of dependence on macrophages (Fig. 4*B*), and EGF and CFS-1 signaling (Fig. 4*C* and *D*), as does the paracrine loop-dependent collection of invasive tumor cells in the *in vivo* invasion assay (10). These results are consistent with previous work showing a correlation between the accumulation of polarized (chemotactic) tumor cells around blood vessels, intravasation and metastasis (7), and the loss of metastatic potential in the absence of tumor-associated macrophages (12).

The role of cell-cell interactions in defining the microenvironment for tumor progression and metastasis has been studied extensively (32). In this regard, macrophages have been hypothesized to play roles in both tumor rejection and increased malignancy (6, 27, 33–35). Part of the reason for this apparent paradox is the lack of direct observations about the behavior and interactions of macrophages with tumor cells *in vivo* that can lead to a mechanistic understanding of the macrophage contribution to malignancy. The new insight resulting from the direct observation of macrophages and their interactions with tumor cells *in vivo* described here is that almost all tumor cell migration and intravasation occur in association with macrophages.

Tumor-associated macrophages have been shown to form clusters in the intratumoral region, and these macrophage dense "hotspots" are correlated with angiogenesis and found to have increased levels of vascular endothelial growth factor (29, 30). However, other groups have reported that the accumulation of macrophages invading carcinomas does not correlate with microvessel density, suggesting that the association of macrophages with blood vessels may contribute to malignancy independently of angiogenesis (36). Here, we describe for the first time that perivascular macrophages of the mammary tumor are associated with tumor cell intravasation in the absence of local angiogenesis.

Previous studies have identified macrophages as a source of EGF, which is chemotactic for tumor cells in mammary tumors *in vivo* (10, 24) and *in vitro* (11, 37). The fact that macrophages are a source of EGF probably explains why tumor cells are polarized toward blood vessels in mammary tumors (9) because these vessels have perivascular macrophages as shown in this study. The involvement of chemotaxis in macrophage-associated tumor cell migration and intravasation is consistent with the gene expression patterns of the invasive population of tumor cells (the invasion signature) collected from mammary tumors as they comigrate with macrophages (38). The "invasion signature" implicates signaling pathways involved in chemotaxis of carcinoma cells (37, 39, 40), consistent with the chemotactic behavior of tumor cells adjacent to macrophages observed *in vivo* in this study and previously *in vitro* (11).

Our results show that the perivascular macrophages of mammary tumors are specifically involved in intravasation. An understanding of how the perivascular macrophage population arises, its relationship to the general population of tissue associated macrophages, and how the interaction of perivascular macrophages with endothelial cells affects vessel integrity and transendothelial migration of tumor cells will be essential in targeting intravasation selectively.

Acknowledgments

Received 5/18/2006; revised 12/18/2006; accepted 12/28/2006.

Grant support: CA100324.

The costs of publication of this article were defrayed in part by the payment of page charges. This article must therefore be hereby marked *advertisement* in accordance with 18 U.S.C. Section 1734 solely to indicate this fact.

We thank the laboratory members and the members of the Gruss Lipper Center for Biophotonics for their contributions to the work discussed in this article.

References

1. Hendrix MJ, Seftor EA, Kirschmann DA, Seftor RE. Molecular biology of breast cancer metastasis. Molecular expression of vascular markers by aggressive breast cancer cells. Breast Cancer Res 2000;2:417–22.
2. Liotta LA, Kohn EC. The microenvironment of the tumour-host interface. Nature 2001;411:375–9.
3. Radisky D, Hagios C, Bissell MJ. Tumors are unique organs defined by abnormal signaling and context. Semin Cancer Biol 2001;11:87–95.
4. Balkwill F, Charles KA, Mantovani A. Smoldering and polarized inflammation in the initiation and promotion of malignant disease. Cancer Cell 2005;7:211–7.
5. Bingle L, Brown NJ, Lewis CE. The role of tumour-associated macrophages in tumour progression: implications for new anticancer therapies. J Pathol 2002;196:254–65.
6. Condeelis J, Pollard JW. Macrophages: obligate partners for tumor cell migration, invasion, and metastasis. Cell 2006;124:263–6.
7. Wyckoff JB, Jones JG, Condeelis JS, Segall JE. A critical step in metastasis: *in vivo* analysis of intravasation at the primary tumor. Cancer Res 2000;60:2504–11.
8. Farina KL, Wyckoff JB, Rivera J, et al. Cell motility of tumor cells visualized in living intact primary tumors using green fluorescent protein. Cancer Res 1998;58:2528–32.
9. Wang W, Wyckoff JB, Frohlich VC, et al. Single cell behavior in metastatic primary mammary tumors correlated with gene expression patterns revealed by molecular profiling. Cancer Res 2002;62:6278–88.
10. Wyckoff J, Wang W, Lin E, et al. A paracrine loop between tumor cells and macrophages is required for

tumor cell migration in mammary tumors. Cancer Res 2004;64:7022–9.
11. Goswami S, Sahai E, Wyckoff J, et al. Macrophages promote the invasion of carcinoma cells *in vitro* via a paracrine loop. Cancer Res 2005;65:5278–83.
12. Lin EY, Nguyen AV, Russell RG, Pollard JW. Colony-stimulating factor 1 promotes progression of mammary tumors to malignancy. J Exp Med 2001;193:727–40.
13. Guy CT, Cardiff RD, Muller WJ. Induction of mammary tumors by expression of polyomavirus middle T oncogene: a transgenic mouse model for metastatic disease. Mol Cell Biol 1992;12:954–61.
14. Ahmed F, Wyckoff J, Lin EY, et al. GFP expression in the mammary gland for imaging of mammary tumor cells in transgenic mice. Cancer Res 2002;62:7166–9.
15. Faust N, Varas F, Kelly LM, Heck S, Graf T. Insertion of enhanced green fluorescent protein into the lysozyme gene creates mice with green fluorescent granulocytes and macrophages. Blood 2000;96:719–26.
16. Sasmono RT, Oceandy D, Pollard JW, et al. A macrophage colony-stimulating factor receptor-green fluorescent protein transgene is expressed throughout the mononuclear phagocyte system of the mouse. Blood 2003;101:1155–63.
17. Motoike T, Loughna S, Perens E, et al. Universal GFP reporter for the study of vascular development. Genesis 2000;28:75–81.
18. Wyckoff J, Segall J, Condeelis J. Single cell imaging in animal tumors *in vivo*. In: Goldman RD, editor. Live cell imaging: a laboratory manual. Cold Spring Harbor (NY): CSHL Press; 2004. p. 409–31.
19. Condeelis J, Segall JE. Intravital imaging of cell movement in tumours. Nat Rev Cancer 2003;3:921–30.
20. Lin EY, Li J, Gnatovskiy L, et al. Macrophages regulate the angiogenic switch in a mouse model of breast cancer. Cancer Res 2006;66:11238–46.
21. Kunkel MW, Hook KE, Howard CT, et al. Inhibition of the epidermal growth factor receptor tyrosine kinase by PD153035 in human A431 tumors in athymic nude mice. Invest New Drugs 1996;13:295–302.
22. Sudo T, Nishikawa S, Ogawa M, et al. Functional hierarchy of c-kit and c-fms in intramarrow production of CFU-M. Oncogene 1995;11:2469–76.
23. Murayama T, Yokode M, Kataoka H, et al. Intraperitoneal administration of anti-c-fms monoclonal antibody prevents initial events of atherogenesis but does not reduce the size of advanced lesions in apolipoprotein E-deficient mice. Circulation 1999;99:1740–6.
24. Wyckoff JB, Segall JE, Condeelis JS. The collection of the motile population of cells from a living tumor. Cancer Res 2000;60:5401–4.
25. Wang W, Wyckoff JB, Wang Y, Bottinger EP, Segall JE, Condeelis JS. Gene expression analysis on small numbers of invasive cells collected by chemotaxis from primary mammary tumors of the mouse. BMC Biotechnol 2003;3:13–25.
26. Austyn JM, Gordon S. F4/80, a monoclonal antibody directed specifically against the mouse macrophage. Eur J Immunol 1981;11:805–15.
27. Leek RD, Harris AL. Tumor-associated macrophages in breast cancer. J Mammary Gland Biol Neoplasia 2002;7:177–89.
28. Dilov P, Dzhurov A. [Histochemical tracing of the iron in the body of piglets injected with an iron-dextran preparation]. Vet Med Nauki 1975;12:70–7.
29. Goede V, Brogelli L, Ziche M, Augustin HG. Induction of inflammatory angiogenesis by monocyte chemoattractant protein-1. Int J Cancer 1999;82:765–70.
30. Salvesen HB, Akslen LA. Significance of tumour-associated macrophages, vascular endothelial growth factor and thrombospondin-1 expression for tumour angiogenesis and prognosis in endometrial carcinomas. Int J Cancer 1999;84:538–43.
31. Lin EY, Gouon-Evans V, Nguyen AV, Pollard JW. The macrophage growth factor CSF-1 in mammary gland development and tumor progression. J Mammary Gland Biol Neoplasia 2002;7:147–62.
32. Chung LW, Baseman A, Assikis V, Zhau HE. Molecular insights into prostate cancer progression: the missing link of tumor microenvironment. J Urol 2005;173:10–20.
33. O'Sullivan C, Lewis CE, Harris AL, McGee JO. Secretion of epidermal growth factor by macrophages associated with breast carcinoma. Lancet 1993;342:148–9.
34. Balkwill F, Mantovani A. Inflammation and cancer: back to Virchow? Lancet 2001;357:539–45.
35. Lin EY, Jones JG, Li P, et al. Progression to malignancy in the polyoma middle T oncoprotein mouse breast cancer model provides a reliable model for human diseases. Am J Pathol 2003;163:2113–26.
36. Davidson B, Goldberg I, Gotlieb WH, et al. Macrophage infiltration and angiogenesis in cervical squamous cell carcinoma—clinicopathologic correlation. Acta Obstet Gynecol Scand 1999;78:240–4.
37. Mouneimne G, Soon L, DesMarais V, et al. Phospholipase C and cofilin are required for carcinoma cell directionality in response to EGF stimulation. J Cell Biol 2004;166:697–708.
38. Wang W, Goswami S, Sahai E, Wyckoff J, Segall J, Condeelis J. Tumor cells caught in the act of invading: how they revealed their strategy for enhanced cell motility. Trends Cell Biol 2005;15:138–45.
39. Ghosh M, Song X, Mouneimne G, Sidani M, Lawrence DS, Condeelis JS. Cofilin promotes actin polymerization and defines the direction of cell motility. Science 2004;304:743–6.
40. Wang W, Goswami S, Lapidus K, et al. Identification and testing of a gene expression signature of invasive carcinoma cells within primary mammary tumors. Cancer Res 2004;64:8585–94.

Direct Visualization of Macrophage-Assisted Tumor Cell Intravasation in Mammary Tumors

Jeffrey B. Wyckoff, Yarong Wang, Elaine Y. Lin, et al.

Cancer Res 2007;67:2649-2656.